Marine Geology 266 (2009) 52–64

Contents lists available at ScienceDirect

Marine Geology

journal homepage: www.elsevier.com/locate/margeo

Diking, young volcanism and diffuse hydrothermal activity on the southern Mid-Atlantic Ridge: The Lilliput field at 9°33′S

K.M. Haase [a,*], A. Koschinsky [b], S. Petersen [c], C.W. Devey [c], C. German [d], K.S. Lackschewitz [c], B. Melchert [c], R. Seifert [e], C. Borowski [f], O. Giere [g], H. Paulick [h]
and M64/1, M68/1 and M78/2 Scientific Parties

[a] Institut für Geowissenschaften der Universität Kiel, Olshausenstr. 40, 24118 Kiel, Germany
[b] School of Engineering and Science, Jacobs University Bremen, Campus Ring 8, D-28759 Bremen, Germany
[c] Leibniz-Institut für Meereswissenschaften, IFM-GEOMAR, Wischhofstr. 1-3, D-24148 Kiel, Germany
[d] Woods Hole Oceanographic Institution, Woods Hole, MA 02543-1050, USA
[e] Institut für Biogeochemie und Meereschemie, Bundesstr. 55, D-20146 Hamburg, Germany
[f] Max-Planck-Institute for Marine Microbiology, Celsiusstr. 1, D-28359 Bremen, Germany
[g] Zoologisches Institut und Zoologisches Museum, Universität Hamburg, Martin-Luther-King-Platz 3, D-20146 Hamburg, Germany
[h] Mineralogisches und Petrologisches Institut, Universität Bonn, Poppelsdorfer Schloss, D-53115 Bonn, Germany

ARTICLE INFO

Article history:
Received 21 January 2009
Received in revised form 7 July 2009
Accepted 17 July 2009
Available online 6 August 2009

Communicated by D.J.W. Piper

Keywords:
South Atlantic
Spreading Centre
vent fauna
basalt

ABSTRACT

Detailed exploration with remotely operated and autonomous deep submergence vehicles has revealed, at 9°33′S, the presence of the southernmost active hydrothermal field known so far on the Mid-Atlantic Ridge. The size of the hydrothermal field, which we have named "Lilliput", is about 1000 m × 250 m. It lies in a water depth of 1500 m on a ridge segment (Segment A3) with considerably thickened crust of 11 km. Four relatively small diffuse vent sites occur on a large young (estimated <100 years old) lava flow, partly covering the flow with hydrothermal Fe-oxide/hydroxide sediments. Based on homogeneous major element compositions of ca. 25 lava samples, this flow covers an area of at least 5 km × 0.6 km. The lava flow erupted from a series of parallel fissures at the western edge of the flow and a volcanic ridge consisting of up to 30 m high pillow mounds. The volcanic ridge probably represents the surface expression of an underlying dike which fed the flow. Several drained lava pond structures were observed within the flow but only one shows hydrothermal activity. The hydrothermal venting and precipitation of abundant Fe-oxyhydroxides appear to be related to the young diking and eruption event and the four different hydrothermally active sites of the Lilliput field lie along and almost equidistant from the eastern flank of the supposed dike. Although a hydrothermal plume some 500 m above the seafloor was found in two consecutive years (2005 and 2006), no high-temperature venting associated with Lilliput has been found, in agreement with findings at other ridges with thick crust such as Reykjanes. High magma supply rate and frequent diking and eruption events may lead to hot hydrothermal vents being rare in slow-spreading segments with thick crust whereas diffuse venting is abundant. Interestingly, the fauna at the Lilliput vents largely consists of small and apparently juvenile mussels (*Bathymodiolus* sp.) and did not show any signs of growth during the four years of continuing observations possibly reflecting pulsing hydrothermal activity.

1. Introduction

Heat was long thought to be transferred from the mantle to the ocean at spreading axes by only two major advective processes — hydrothermalism and magmatism. At fast-spreading ridges these processes are known to be generally intimately linked, both spatially and temporally (e.g. Haymon et al., 1991). At slow-spreading ridges, however, periods of volcanic activity may be followed by long episodes of tectonic activity. The occurrence of off-axis (e.g. Melchert et al., 2008) and serpentinite-hosted (Kelley et al., 2002) hydrothermal systems implies a less clear-cut link between magmatism and hydrothermalism and that tectonic mass movement also leads to significant heat transfer. At fast-spreading ridges much of the hydrothermal activity appears to be connected to dike intrusion events with or without eruption of lava at the surface (Delaney et al., 1998). On the other hand, many of the hydrothermal fields on slow-spreading ridges appear to occur above melt lenses in the crust with fluid circulation developing along deep-reaching fractures (e.g. Singh et al., 2006).

Some areas of the global ridge system are known, from geophysical measurements, to have thickened crust and yet very few hydrothermally

* Corresponding author. Present address: GeoZentrum Nordbayern, Universität Erlangen-Nürnberg, Schlossgarten 5, D-91054 Erlangen, Germany.
E-mail address: haase@geol.uni-erlangen.de (K.M. Haase).

0025-3227/$ – see front matter © 2009 Elsevier B.V. All rights reserved.
doi:10.1016/j.margeo.2009.07.012

active sites have been found on such ridges. For example, along a 600 km long section of the Reykjanes Ridge, whose 10-km thick crust is thought to result from the influence of the Iceland melting anomaly, detailed water sampling (German et al., 1994) found only one hydrothermal vent (global studies show that, on average, between one and three sites per 100 km of ridge length might be expected, depending on magmatic budget, Baker and German, 2004). As the amount of heat which has to be removed from the crust should scale with thickness, this apparent lack of hydrothermal venting on thickened crust is surprising. The magmatic and hydrothermal processes at slow-spreading ridge segments with thick crust are not well understood but several mechanisms have been proposed to explain why and how thickened crust (especially in its deeper parts) may be cooled without high-temperature venting at the seafloor (e.g. Baker and German, 2004). For example, it has been suggested that thick and hot crust may not develop the deep faults necessary to allow deep water circulation (e.g. Devey et al., in press) or that the presence of melt lenses in the shallow crust inhibits the deep intrusion of water into the crust (German et al., 1994; Chen, 2003).

Here we report details of the most southerly known hydrothermal system on the MAR which was found and studied during three cruises with FS *Meteor* in 2005, 2006 and 2009, and show it to be closely related to recent volcanic activity. We describe the volcano-tectonic setting, the hydrothermal sites and deposits as well as the biology of the low-temperature field which occurs on crust which is about 11 km thick. Due to the high magma production the crust resembles an intermediate-spreading melt-anomaly influenced ridge with a volcanically active axial high rather than a deep rift valley. We suggest that the diffuse venting is the product of a diking and eruptive event. Hydrothermal activity since the event seems to have waned as we see large extinct hydrothermal mounds close to the areas of present-day weak low-temperature venting. Furthermore the southerly location of this field has important biogeographical implications and we explore the implications of the fauna discovered for the discussions on barriers to faunal exchange in the deep ocean.

2. Geological setting of the study area

The study area is located on the MAR between the Ascension and the Bode Verde fracture zones (Fig. 1a) where the full spreading rate is 32–33 mm/yr (DeMets et al., 1994). Geophysical studies of the region have previously established that the MAR between 7 and 12°S consists of four segments which have been termed A1 to A4 (Minshull et al., 1998; Bruguier et al., 2003). Bruguier et al. (2003) show that significant gravity anomalies occur along segments A1 to A4 which may be attributed to crustal thickness variations rather than thermal effects of a mantle plume. The study presented here concentrates on Segment A3, one of the two central segments that have experienced ridge jumps in the last 1 Ma. Segment A3 is the shallowest of the four segments and is characterized by a 70 km long axial high with two large off-axis seamounts located east of the ridge (Brozena, 1986). It has a significantly thickened crust of about 11 km based on gravimetric modelling (Bruguier et al., 2003) — a seismic study revealed a thickness of ~10 km for the segment A2 further north (Minshull et al., 1998). The morphology of the spreading axis on segment A3, with its 2 to 4 km wide rift valley (Figs. 1b and 2) rather than the approx. 30 km wide and much deeper rift valley typical for the slow-spreading MAR, is similar to that of volcanically and hydrothermally active intermediate-spreading ridges like the Galapagos Spreading Centre at 86°W (Corliss et al., 1979; Shank et al., 2003).

3. Observation and sampling methods

The area between 8°S and 10.5°S was studied during three cruises with FS *Meteor* (M64/1 in April/May 2005, M68/1 in May 2006 and M78/2 in May 2009) in order to find signs of hydrothermal activity and to determine the relationship between volcanic and hydrothermal processes. The first two cruises carried out conductivity–temperature–depth (CTD) casts, sampling of rocks using a wax corer and a TV-guided grab, and work with a remotely operated vehicle (ROV). Sampling sites are shown in Fig. 2. CTD casts were carried out using a Sea-Bird Electronics, Inc. SBE 911plus system, additionally equipped with a Miniature Autonomous Plume Recorder — MAPR (Baker and Milburn, 1997). The underwater unit was attached to a SBE 32 carousel water sampler with 22 Niskin bottles. Additionally, during rock coring along the axis, a MAPR was also attached to the cable about 80 m above the wax corer in order to explore for hydrothermal plumes. The hydrothermal fields were observed and sampled using the "Quest" and "Kiel6000" remotely operated vehicles equipped with several still and film cameras and two manipulating arms. The ROVs were navigated using a self-calibrating acoustic IXSEA GAPS USBL positioning system allowing positioning to be accurate to within ca. 1% of water depth (in the case of Lilliput conservatively estimated as an error of 20 m). The ROV arms were used to sample hydrothermal precipitates e.g. from vents, biological samples, and to pick up lava samples. Lava and biological samples were also recovered in several TV-guided grabs used to sample hydrothermal precipitates. The TV-guided grab was deployed from the ship without extra navigation and closed when hydrothermal structures were observed through the camera system. In 2006 the AUV ABE and in 2009 the AUV "ABYSS" were used to map the bathymetry of parts of the study area in detail — one of these maps is shown in Fig. 3. Detailed bathymetric data of the Lilliput area was obtained by the autonomous underwater vehicle AUV ABYSS from IFM-GEOMAR using a 400 kHz Reson SeaBat 7125 which was operated with 512 beams in an equal area mode. The AUV was flown at 3 kn in a constant water depth of 1440 m with a trackline spacing of 80 m. ABYSS was navigated autonomously using a combination of an inertial navigation system (Kearfott T-24 INS) and a long baseline acoustic navigation by computing its range to two moored acoustic transponders (located 30 m above seafloor) yielding a horizontal navigation accuracy of ± 5 m. Vertical accuracy of the vehicle is better than 1 m, while vertical resolution at the seafloor is better than 10 cm. Postprocessing of the bathymetric data was performed using the software PDS2000 from Reson. Circular interpolation using a 0.7 m grid cell size was used to calculate the map.

Hydrothermal fluids were sampled in situ using the remotely controlled flow-through Kiel Pumping System (KIPS-3) which was mounted on the tool sled of the ROV and which has been described previously (Haase et al., 2007). Dissolved hydrogen and methane, the pH as well as Cl, Mg, Si, and Fe concentrations of the hydrothermal fluids were determined on samples from the KIPS by applying methods described in detail in Haase et al. (2007). Hand-picked glass from the lava samples was analysed by electron microprobe (EMP) at the Institut für Geowissenschaften of the Christian-Albrechts-Universität Kiel, using a JEOL Superprobe 8900 and standard wavelength-dispersive techniques. The instrument was operated at an accelerating voltage of 15 kV and beam currents of 20 nA. The beam diameter during standardisation and measurement was set at 12 µm. Counting times on peaks and background varied depending on the element analysed, and were 20 s for all major elements except Na_2O which was analysed with peak counting times of 10 s. Background counting times were always half of peak counting times. Each glass sample was analysed 8 to 10 times and the average was calculated.

4. Results

4.1. Hydrothermal plume exploration and water chemistry

Fourteen regional CTD and water sampling stations (Fig. 4, Table 1) carried out during cruise M64/1 on segment A3 helped to define the hydrothermally active area. Additional 14 CTD and water sampling stations in the study area and especially further south were carried out during cruise M62/5 in December 2004 (Fig. 4). No signs of

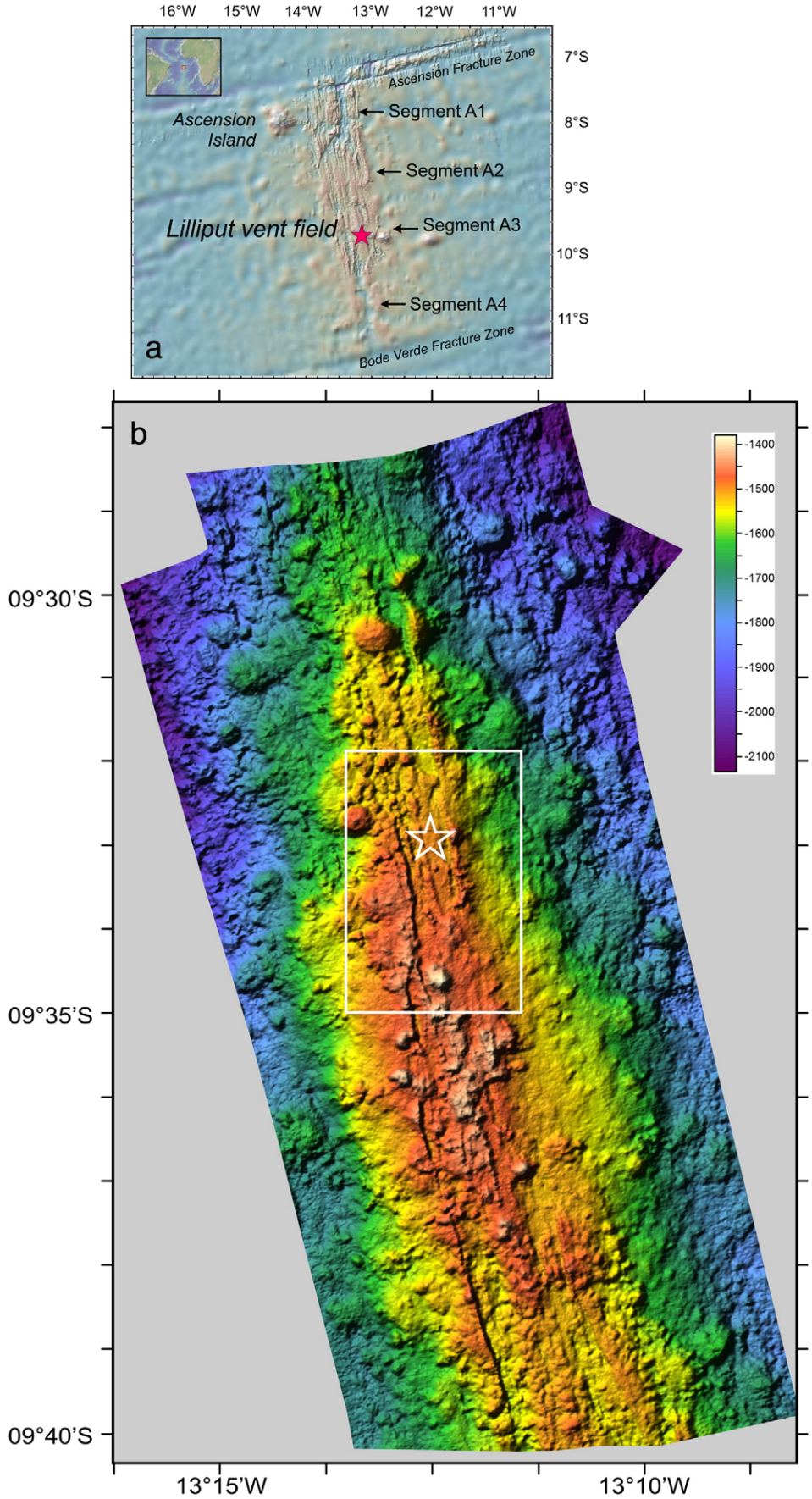

Fig. 1. a) Location map of the Mid-Atlantic Ridge near 9°33′S. b) Multi-beam bathymetric map of the ridge segment A3 showing the location of the active Lilliput hydrothermal field. Bathymetric data was collected using a Kongsberg Simrad EM 120 systems with12 kHz, 2×45° opening angle and 191 beams per ping corresponding to a theoretically resolution of ~30×30 m. Ship's speed was set to 8 kn during surveys. The area within the white box is enlarged in Fig. 2.

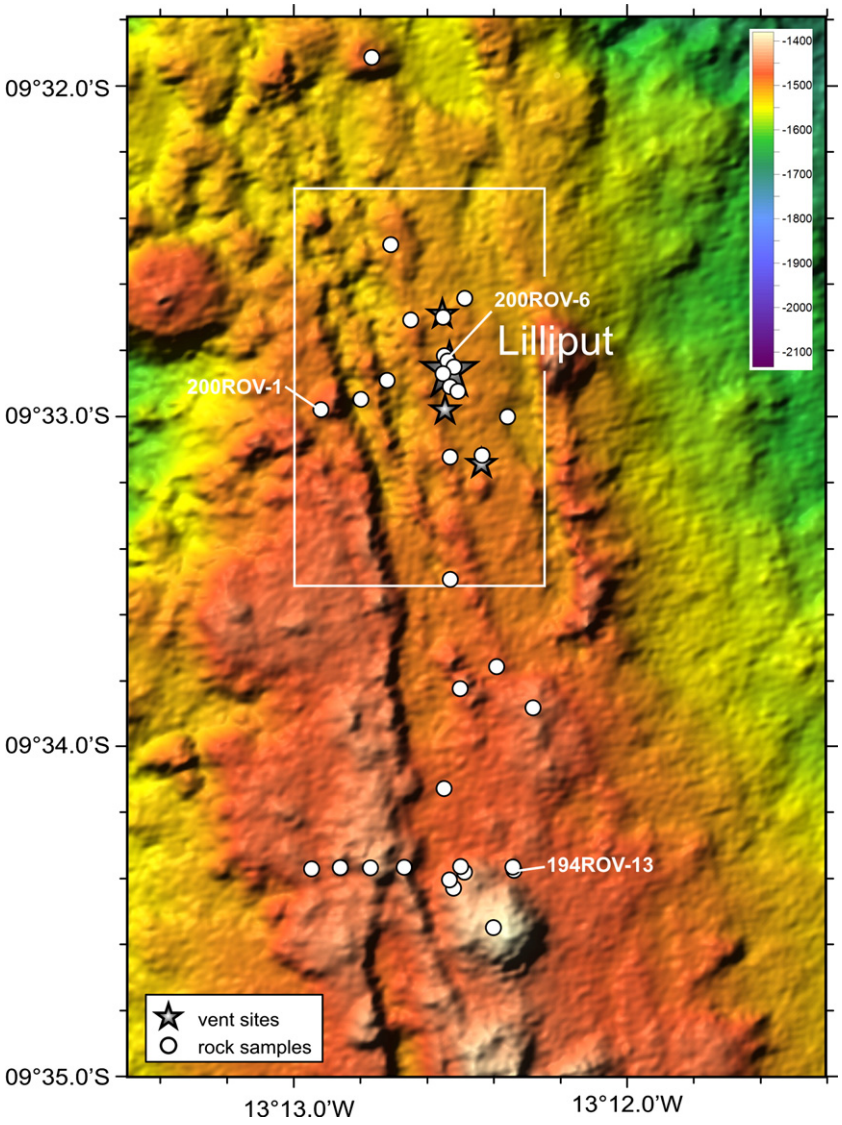

Fig. 2. Enlarged bathymetric map of the volcanically active region of the Mid-Atlantic Ridge close to the Lilliput hydrothermal field with the vent sites shown as stars. Also shown are rock sample locations obtained by ROV, wax corer, and dredge. The white box outlines the area of detailed AUV mapping presented in Fig. 3.

hydrothermal activity were found on the northern part of this segment but close to the segment centre in the area between 9°27′S and 9°34′S, we observed high concentrations of CH_4 up to 53 nmol/l relative to a background of <0.5 nmol/l either close to the seafloor (1500 m) or at around 1000 m water depth (Fig. 5a) The Mn and Fe analyses of water samples show the near-seafloor CH_4-anomaly to be associated with an Fe peak in some profiles (e.g. 208CTD) while Mn appears to be decoupled from these two (Fig. 5b). Iron concentrations are widely used as a hydrothermal tracer in plumes (German and Von Damm, 2003). The increased concentrations of Fe and/or CH_4 were interpreted as signs of hydrothermal plumes although no turbidity or temperature anomalies were detected. The occurrence of anomalies on and ~500 m above the seafloor suggests at least two different hydrothermal plumes in the water column.

4.2. Observations at the hydrothermal sites

In total four low-temperature venting sites in the Lilliput area have so far been discovered (see Fig. 3). These newly-discovered sites lie in water depths of ca. 1500 m on the northern flank of the Segment A3 axial high (minimum water depth on Segment A3 is 1200 m). The plate boundary at the Lilliput hydrothermal field is characterized by a ca. 800 m-wide axial trough bounded by faults with scarps of 10 to 20 m height (Fig. 3). The lavas outside the trough are heavily sedimented whereas volcanic rocks between the fault scarps show no pelagic sediment cover. A 100 to 200 m wide ridge consisting of numerous small pillow mounds up to about 30 m high lies in the centre of the trough (Figs. 2 and 3). A relatively flat area some 300 to 400 m wide lies east of the volcanic ridge (Fig. 3) and consists mainly of young lobate and pillow lavas with abundant collapse structures such as skylights, lava pillars and collapsed roofs. This flat area shows an irregular boundary of a lava flow front to the east and is about 20 m shallower than the rest of the floor of the axial trough. The hydrothermally active sites lie along the eastern flank of the volcanic ridge (Fig. 3; Table 2). Venting is diffuse with fluid temperatures of 4.8° to 15.8 °C measured in situ at the vents (Table 2). The fauna around most vents is visually dominated by small mussels which at a first glance resembled *Bathymodiolus puteoserpentis* from the northern MAR and was preliminarily assigned to *Bathymodiolus* sp. until detailed taxonomic and genetic analysis. The unusual absence of large individuals led to the naming of the field (see "Gulliver's Travels", Swift, 1726). The *Main Lilliput* low-temperature site (Fig. 3) consists of abundant, semi-lithified Fe-oxyhydroxide crusts covering an area of approximately 100 m × 40 m (Fig. 6a, b and c). In 2005 and 2006, colonies of

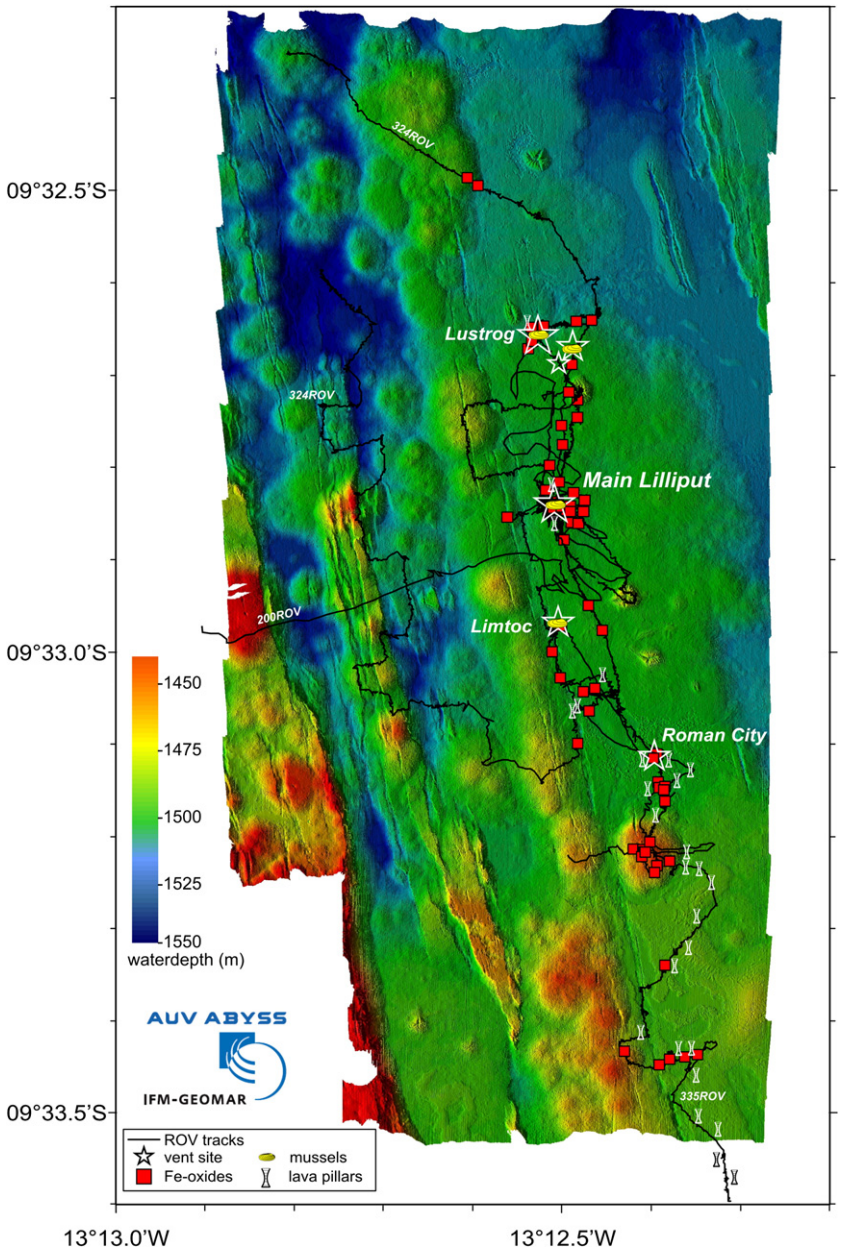

Fig. 3. Detailed bathymetric map based on AUV high-resolution multi-beam mapping (Reson Seabat 7125) showing the faulted western rift flank and the volcanic ridge consisting of a row of pillow mounds. Numerous parallel fissures which also occur east of the ridge. Note the about 1500 m deep and flat area east of the volcanic ridge which is interpreted as a young lava flow with clear flow fronts to the about 20 m deeper rift valley to the east. The four diffuse hydrothermal vent sites occur within this lava flow and about equidistant to the ridge. The lines show the ROV tracks and the symbols denote selected ROV dive observations. Selected ROV tracks mentioned in the text are labeled.

small *Bathymodiolus* sp. mussels formed linear and patchy structures which follow venting along cracks and contacts in the underlying basalt pillows (Fig. 6d). In 2009, the populations had considerably grown and small mussels blanketed the pillows in patches of several square meters. The *Limtoc* site (Fig. 3) resembles the Main Lilliput site in structure and occurrence of vents and fauna. The highest temperature of 15.8 °C and the highest H_2S concentrations of 341 mmol/l for the whole field as well as a relatively low pH of 6.2 were measured in fluids from one of the Limtoc vents (Table 2). The *Roman City* site (Fig. 3) is characterized by two distinct types of hydrothermal features; (1) large mounds of orange-coloured Fe-oxyhydroxide hydrothermal sediments which, although testifying to extensive hydrothermal activity in the past, showed no evidence for present-day venting (Fig. 6e) and (2) diffuse venting associated with high-porosity lava-sheet fields showing drain out roof- and column structures (Fig. 7a). The *Lustrog* site is characterized by pillow lavas and venting of milky water from some collapsed pillows. Temperature measurements gave values of up to 7.0 °C. This site shows venting in two areas separated by a fissure from which lava lobes radiate, suggesting that the fissure was their eruption source. The fauna contains mussel colonies and abundant sponges *Eucheliplumapristina* (Fig. 6f) growing on top of the pillows. In 2009, extensive colonies of young mussels blanketing the pillows were observed NE of Lustrog. Additional sites of Fe-oxyhydroxide precipitation without clear evidence for venting occur all along the eastern flank of the volcanic ridge and seem to continue further to the south. Some of these are clearly older and are sediment dusted, while others show fragile structures without any sediment cover.

The Mg concentrations of the emanating fluids are slightly lower than those in seawater (Table 2) indicating that the diffuse fluids consist of a few percent of hydrothermal end-member fluid (presumed to be Mg-free) mixed with seawater. The fluids are slightly

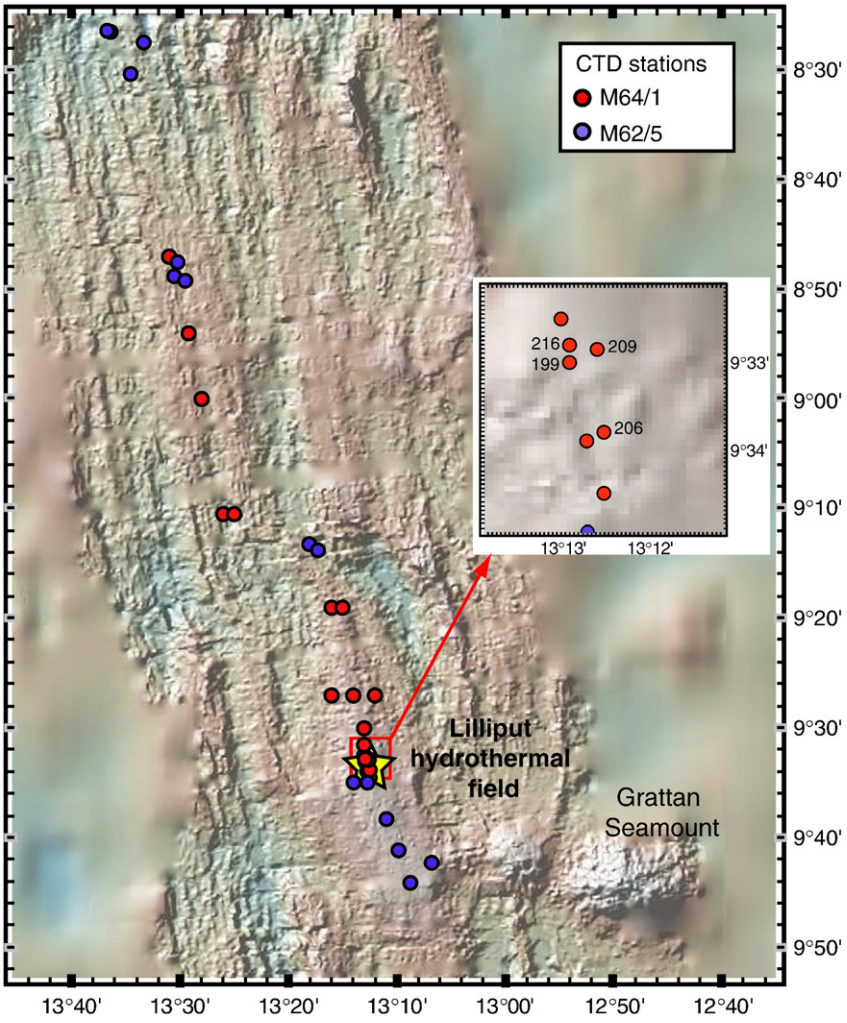

Fig. 4. Bathymetric map of the study area showing the location of the CTD stations carried out during M62/5 and M64/1 leading to the discovery of the Lilliput diffuse vent field. The inset shows the detailed location of the CTD stations close to the Lilliput field presented in Fig. 5.

acidic (a minimum pH of 5.9 was measured on board) and reducing. The maximum silica concentration in the Lilliput fluids is 0.54 mmol/l, i.e. significantly increased relative to the content of <0.01 mmol/l in the surrounding seawater (Table 2). Dissolved Fe concentrations range between 0.1 and 43 µmol/l and generally correlate with fluid temperatures, with the highest Fe contents occurring in the Limtoc site sample with the lowest pH. Fluids sampled directly from these vents with the KIPS system have high CH_4 concentrations and very low H_2/CH_4 ratios (Table 3).

Observations and the sampling of the mussels around the vents showed an unusually strong bias towards small specimen at the Lilliput field (Fig. 6c, d, and f). About 80% of the mussels sampled on May 18th and 27th 2005 are less than 1.5 cm in length compared to only 1.5% larger than 6.5 cm (number of measured specimens $n=1062$). Sampling yielded mainly post-larval young mussels (0.5 mm in size). In 2009, the population size had considerably grown and the size frequency distribution again revealed that 90% of the population was less than 3 mm long and is therefore suggested to be less than one year old. This indicated that the supply with settling juveniles had been continuous during the preceding months. The largest specimen sampled measured 58 mm shell length. The amount of shells of dead adults was in contrast low and they were only found where no active venting was observed. Their calcium carbonate was often dissolved and only their periostracum was left (Fig. 6b). Shrimps (mainly *Rimicaris exoculata*) and bythograeid crabs are rare and only a few specimens were observed directly at the source of venting. Additionally, scavengers like the snail *Phymorhynchus* and worms were observed. Bacterial mats were also observed within cavities of the Fe crusts (Fig. 6f). In the vicinity of the mussel beds single specimens of the carnivorous sponge *Eucheliplumа pristina* (Topsent, 1909) sit on the Fe-oxide coated pillows (Fig. 6f).

4.3. Volcanic setting and composition of the host lavas

The faults bounding the axial trough at 9°33′S mark a clear change in lava age — our ROV observations west of the axial valley scarp (as at station 200ROV-1, Fig. 2, for example) show the lavas covered with large sediment pockets and cut by normal faults with abundant talus piles. In contrast, the four Lilliput hydrothermal sites are situated within the axial trough on pillow, lobate and occasional sheet lavas with a relatively young appearance (Fig. 7). Although the sedimentation rate in this area of the southern MAR is about 32 mm/kyr (Ruddiman and Janecek, 1989) there is no pelagic sediment on or between the lavas (Fig. 7). A comparison of these lavas with other sites of recent volcanic activity on the global ridge system (Chadwick and Embley, 1994; Sturm et al., 2000) suggests eruption ages of less than 100 years. The Lilliput hydrothermal field is clearly situated within the volcanically active zone of the Mid-Atlantic Ridge.

The high-resolution AUV bathymetry reveals that the hydrothermal vents lie on a ca. 20 m-thick lava flow with eastward-directed flow fronts (Fig. 3). Three larger volcanic tumuli exist on the surface of this lava flow. The lava flow probably erupted from the volcanic ridge

Table 1
CTD stations in segment A3 and gas contents of water samples from different water depths as determined on board during the M64-1 cruise.

Station #	Lat. (°S)	Long. (°W)	Bottle #	Water depth (m)	CH_4 (nM)	H_2 (nM)
186CTD	9.317	13.267	19	1101	27.90	34.99
			17	1178	0.43	11.90
			15	1192	0.40	10.58
			13	1261	0.34	11.24
			9	1299	0.27	10.82
			7	1618	0.44	9.03
			5	1772	0.41	
			3	1836	0.51	8.82
			1	1884	0.70	10.69
187CTD	9.317	13.250	7	451	0.27	9.34
			5	1202	0.40	30.77
			3	1295	0.40	6.32
189CTD	9.450	13.233	19	978	0.76	7.10
			17	1051	6.25	
			15	1106	0.51	18.84
			13	1139	0.33	3.32
			9	1186	52.67	1.54
			7	1298	0.48	1.93
			5	1392	24.86	24.96
			3	1446	0.38	7.45
190CTD	9.450	13.267	7	995	1.03	12.52
			5	1046	0.52	9.00
			3	1098	0.49	1.95
			1	1200	0.56	4.30
191CTD	9.450	13.200	12	1050	0.75	4.61
			9	1100	0.46	2.88
			7	1150	4.91	13.61
			5	1200	0.25	18.69
			3	1250	0.46	8.23
			1	1301	0.41	14.54
192CTD	9.500	13.217	21	1076	0.37	11.24
			19	1175	53.79	9.02
			17	1250	0.49	9.00
			15	1325	0.52	15.36
			13	1375	0.36	7.66
			9	1424	0.67	5.21
			7	1480	0.78	10.23
			5	1537	0.37	32.49
			3	1600	0.51	8.09
			1	1620	0.53	3.39
193CTD	9.542	13.217	9	1075	35.92	5.30
			7	1173	6.92	6.73
			5	1325	19.97	7.85
			3	1375	16.42	13.23
			1	1425	47.27	29.03
195CTD	9.575	13.208	19	925	0.56	0.92
			17	1024	1.17	
			15	1075	0.68	3.10
			13	1108	0.59	4.26
			9	1173	0.54	11.60
			7	1198	0.56	16.81
			5	1230	0.90	2.37
			3	1233	0.92	44.34
			1	1397	1.75	29.23
196CTD	9.525	13.217	17	1025	57.49	1.70
			15	1100	56.26	3.03
			13	1175	0.75	3.77
			9	1225		5.29
			7	1300		7.54
			5	1425		10.72
			3	1475	0.53	12.01
			1	1530	0.91	4.04
197CTD	9.565	13.212	13	1100	1.07	15.99
			9	1175	0.39	1.96
			7	1229	0.33	1.15
			5	1302	0.62	10.49
			3	1360	0.71	5.62
			1	1430	0.77	6.39
199CTD	9.550	13.215	19	900	6.94	13.40
			17	975	3.29	3.49
			15	1041	52.76	1.91
			13	1114	1.20	2.14
			9	1186	0.42	6.09
			7	1244	0.68	5.83
			5	1308	2.44	0.42
			3	1395	41.23	3.85
			1	1450	3.69	4.29
206CTD	9.563	13.208	23	940	0.07	19.50
			21	1000	8.63	9.94
			19	1043	3.04	1.08
			17	1100	0.07	12.82
			15	1150	0.65	21.15
			13	1200	0.30	21.96
			11	1250		3.42
			9	1300	0.46	1.83
			7	1350	0.89	3.66
			5	1389	0.97	16.81
			3	1429		2.88
			1	1469		3.63
208CTD	9.548	13.210	17	1000	0.47	14.66
			15	1050	6.76	20.44
			13	1100	0.26	19.57
			11	1210	0.06	16.19
			9	1290	0.04	16.70
			7	1380	0.48	14.08
			5	1410	0.16	15.26
			3	1456	0.09	32.86
			1	1494	17.40	7.26
216CTD	9.547	13.215	23	900	31.01	2.13
			21	950	12.01	1.30
			19	1000	0.87	0.76
			17	1040	17.70	0.96
			15	1074	0.81	0.69
			13	1130	0.53	0.91
			11	1200	0.61	3.14
			9	1270	4.65	1.24
			7	1350	0.88	1.13
			5	1410	0.78	1.22
			3	1476	0.20	0.29
			1	1505	0.42	0.32

which lies immediately to the west, most likely from a series of narrow parallel volcanic fissures occurring within the pillow mounds and east of the volcanic ridge. Some of these fissures show drainback features of the lava, evidence that they were the eruption feeders. In the area of the Lilliput hydrothermal field only few young pillow mounds related to this most recent eruption occur west of the volcanic ridge (Fig. 3). This flow is also distinguishable by being almost totally devoid of fractures — a further indication of its young age.

Thirty-nine samples of pillow and sheet lava fragments were recovered in the vicinity of the Lilliput hydrothermal field with ROV, TV-guided grab, and wax corer (Fig. 2). All samples are relatively young with unaltered glass rims although they are close to hydrothermal vents. With the exception of one sample (200ROV-6) all glasses from the young lavas surrounding the Lilliput hydrothermal field but also to the south and north of the field fall into a narrow compositional range of MgO 5.2 to 6.4 wt.% and K/Ti of 0.20 to 0.26 (Table 4 and Fig. 8). In contrast, the lavas sampled by ROV outside of the field of recent lavas have a much greater range of K/Ti and mostly higher MgO contents (Fig. 8a). The most MgO-rich sample (194ROV-13) within the relatively homogeneous group of recent lavas is from a young-looking sheet flow from a collapse structure closely associated with pillow lavas at the southern part of the studied area (Fig. 2).

5. Discussion

5.1. Distribution of hydrothermal activity and precipitates

The young-looking pillow lava flow is covered in many regions by thick Fe-oxyhydroxide crusts (Fig. 6a) and many lava surfaces show

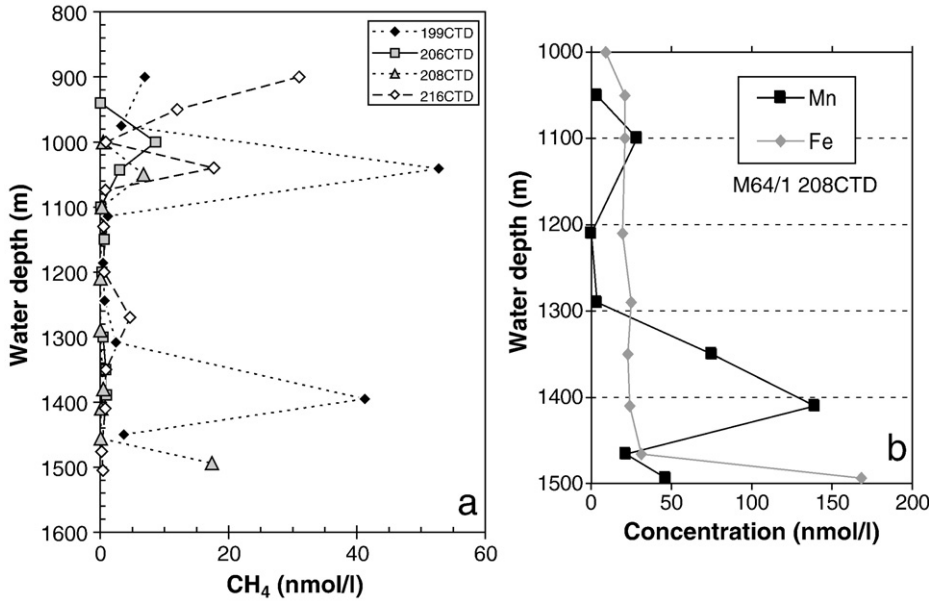

Fig. 5. Profiles of (a) CH_4 concentrations at CTD stations 199CTD (9°33.00′S; 13°12.90′W), 206CTD (9°32.70′S; 13°12.50′W), 208CTD (9°32.85′S; 13°12.58′W), and 216CTD (9°32.80′S; 13°12.90′W), and (b) Mn and Fe concentrations at station 208CTD determined on board above the Lilliput vent field showing anomalies both at the bottom and about 500 m above the seafloor. Note that Mn shows anomalies at the same depths as CH_4.

Fe-oxyhydroxide staining. Hydrothermal sediments also occur in collapse pits (Fig. 6b). Several centimetre thick orange and rarely greenish precipitates consisting of Fe-oxyhydroxides cover the basalts within 10 s of metres of the vents at the Main Lilliput site. Similar material is typical for low-temperature venting on other parts of the mid-ocean ridge (German and Von Damm, 2003). Further to the south and around the Roman City site, significantly larger (600 m × 200 m) and, because they usually cover the entire volcanic substrate, likely thicker hydrothermal deposits have been found. The occurrence of larger extinct hydrothermal mounds (Fig. 6e) and the presence of old mussel shells with Mn-oxide coatings in these areas (Fig. 7b) suggest previous, possibly more intense, episodes of hydrothermal activity. This intense hydrothermal activity most likely directly followed the eruption of the lavas and was related to the cooling of the thick lava flow as has been observed along a recent lava flow on the Cleft segment of the Juan de Fuca Ridge (Embley and Chadwick, 1994). In contrast, the on-going diffuse hydrothermal activity is probably driven by heat from the dike that fed the eruption.

5.2. Hydrothermal plume compositions: evidence for venting with different temperatures?

The localized CH_4 and Mn anomalies immediately above the seafloor (Fig. 5) are probably due to the venting of low-temperature fluids from Lilliput as they occur directly above the vent field. The signal of this venting can be traced only less than 2000 m from the known vent sites. In contrast, another CH_4 anomaly observed in many CTD profiles at around 1000 m water depth (see Fig. 5) is not likely to originate from diffuse venting because the only seafloor at that depth is more than 20 km distant to the east. We therefore favour a high-temperature source producing a buoyant hydrothermal plume as an origin of this CH_4 anomaly. This is supported by the chemical composition of the Lilliput fluids, which clearly shows that they contain a high-temperature component (with low Mg, low pH, high dissolved Si) which has been diluted with ambient seawater, presumably in the shallow sub-surface. The variability of H_2/CH_4 ratios between 1 and 460 (Table 1) but relatively constant maximum CH_4 concentrations (ca. 50 nM) in the ±1000 m plume between different CTD stations may suggest that the plume stem is relatively distal and that oxidation, particularly of H_2, is leading to these variations. For example, a study of an event plume after an eruption on Gorda Ridge revealed that H_2 concentrations decreased from 47 nM in the event plume to 6.2 nM one month later (Kelley et al., 1998) supporting a fast decrease of H_2 concentrations in the water column. The shallow hydrothermal signal was found both in 2005 and 2006 implying a relatively stable plume in the water column. At a depth of 1400 to 1500 m, the boiling temperature for seawater is around 340–350 °C (Bischoff and Rosenbauer, 1984) and small variations in temperatures around 350 °C could lead to significant changes in the concentrations of strongly temperature-dependent elements such as Fe and H_2. No

Table 2
Locations of the vent sites of the Lilliput hydrothermal field as well as temperatures, pH, and compositions of some of the fluids.

Site name	Latitude; longitude	Water depth	Sample	Temperature	pH at 25 °C	H_2S mmol/l	Mg mmol/l	Cl mmol/l	Si mmol/l	Fe mmol/l
Lustrog	9°32.66′S; 13°12.53′W	1501 m	M68/1 41ROV-6	6.6 °C	6.6	29	50.0	553	0.134	8.9
	9°32.65′S; 13°12.52′W	1505 m	M68/1 41ROV-10	7.0 °C	6.6	18	51.5	555		
			M68/1 41ROV-12	6.5 °C	6.9	45	49.1	553	0.135	3.2
Main Lilliput	9°32.84′S; 13°12.51′W	1495 m	M68/1 41ROV-5	4.8 °C	7.2	15	52.2	552	0.061	0.12
			M64/1 200ROV B11	5.1 °C	6.4		51.0	537	0.36	0.61
			M64/1 200ROV B12	n.d.	6.5		52.5	544	0.32	0.69
			M64/1 200ROV B13	n.d.	6.4		51.8	543	0.30	0.75
			M64/1 200ROV B14	n.d.	n.d.		52.8	541	0.30	0.63
Limtoc	9°32.97′S; 13°12.50′W	1494 m	M68/1 39ROV-4	15.8 °C	6.2	341	52.1	537	0.542	12.7
Roman Ruins	9°33.11′S; 13°12.40′W	1495 m	M68/1 70ROV-2	8.5 °C	5.9	4	51.6	553	0.211	43.3

n.d. = not determined.

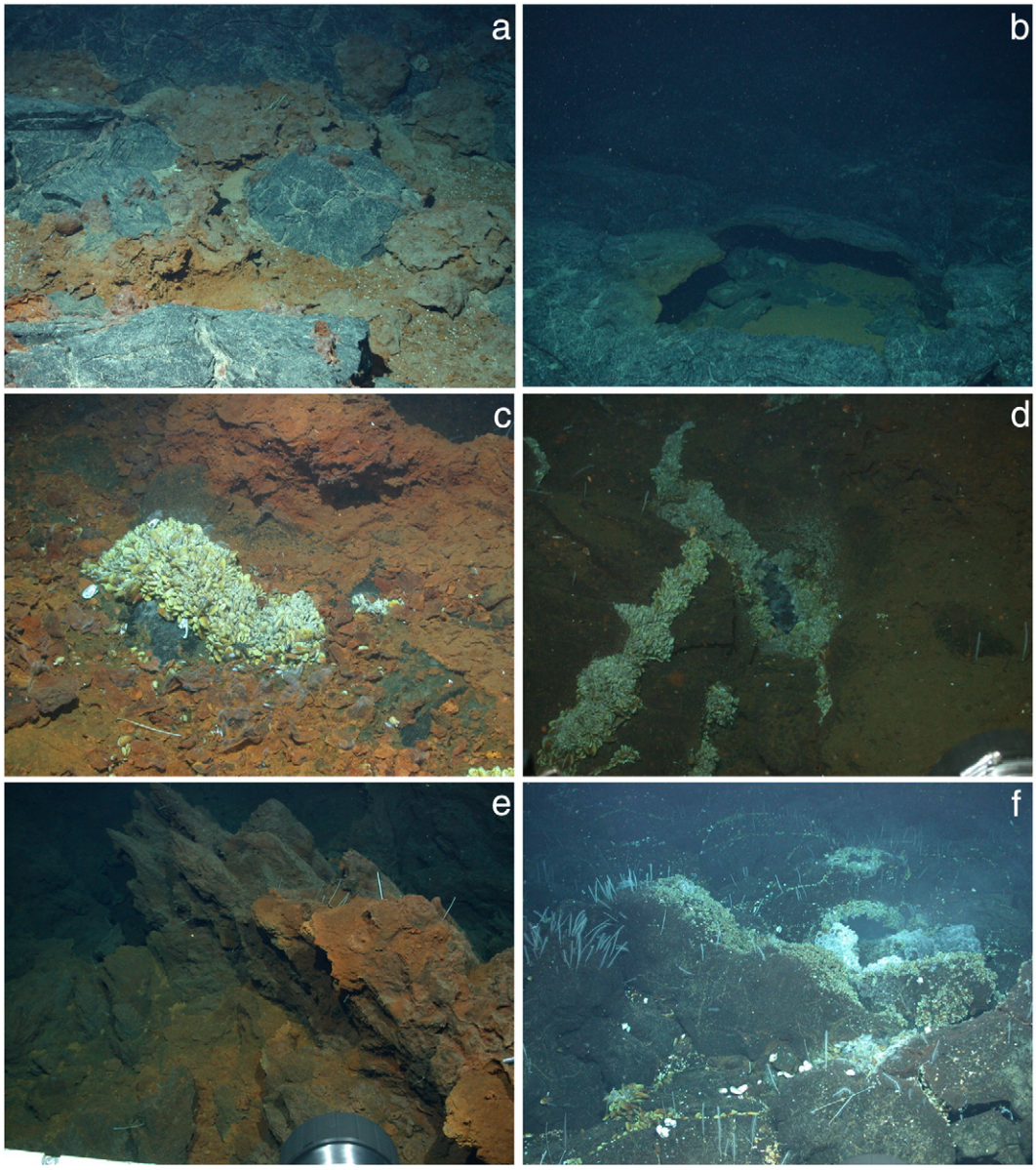

Fig. 6. Photographs of (a) the hydrothermal Fe-oxyhydroxide deposits (Main Lilliput site). Field of view: ~1.5 m, (b) a skylight in the lava flow filled with hydrothermal sediments (Main Lilliput site). Field of view: ~3 m, (c) and (d) small mussel (*Bathymodiolus puteoserpentis*) beds along cracks and vents emanating hydrothermal fluids (Main Lilliput site). Field of view: ~2 m in both images, (e) massive Fe-oxyhydroxide crusts (Roman City site). Field of view: ~2 m, and (f) mussel beds and sponges *Eucheliplума pristina* (Lustrog site). Field of view: ~5 m. Copyright MARUM, University of Bremen, Germany.

sign of a hot vent or bouyant plume stem close to the Lilliput field was found during the extensive CTD and Eh mapping program using ABE in 2006, although this survey was carried out much deeper than the plume level of about 1050 m depth. Likewise, ship-based CTD stations carried out in 2004 close to the seamounts east of the Lilliput field did not find any sign of hydrothermal activity (Devey et al., 2005). Consequently, the origin of the shallow anomaly remains enigmatic.

5.3. The volcano-tectonic setting of the vents

The similarity of the lava appearance from camera observations and their narrow compositional range suggests that all lavas in the axial trough between about 9°34.5′S and 9°31.9′S (Figs. 2 and 8b) formed during one large eruptive event. The fresh lavas probably erupted from the fissures adjacent to the ≥3 km long volcanic ridge in the west of the axial trough and thus may have slightly different eruption sites. The lava flow apparently covers an area about 5 km long and up to 600 m across axis. Assuming a thickness of 20 m for the lava flow from the height above the surrounding floor of the rift valley (Fig. 3) we estimate an eruptive volume of perhaps 60×10^6 m^3 comparable to lava flows from other parts of the spreading axis system, in particular the Serocki Volcano eruption (Rubin et al., 2001). The homogeneity index HI for the Lilliput lavas yields a value of 5.14 (Table 4), significantly higher than that of the Serocki Volcano eruption but generally supporting more heterogeneous compositions in large volume eruptions (Rubin et al., 2001). However, the small range of the MgO contents in the glasses suggests that only minor amounts of differential crystal fractionation of olivine and plagioclase within the magma body occurred prior to eruption.

The parallel alignment of the volcanic cones forming the volcanic ridge, the fissures, and the hydrothermal venting sites all within the axial trough and within the extensive recent lava flow field suggests that they are genetically related. The row of volcanic shields and pillow mounds up to 30 m high in the centre of the volcanically active zone (Fig. 2) probably reflects the presence of a sub-surface dike from which the lava mounds and the lava flow erupted (Head et al., 1996).

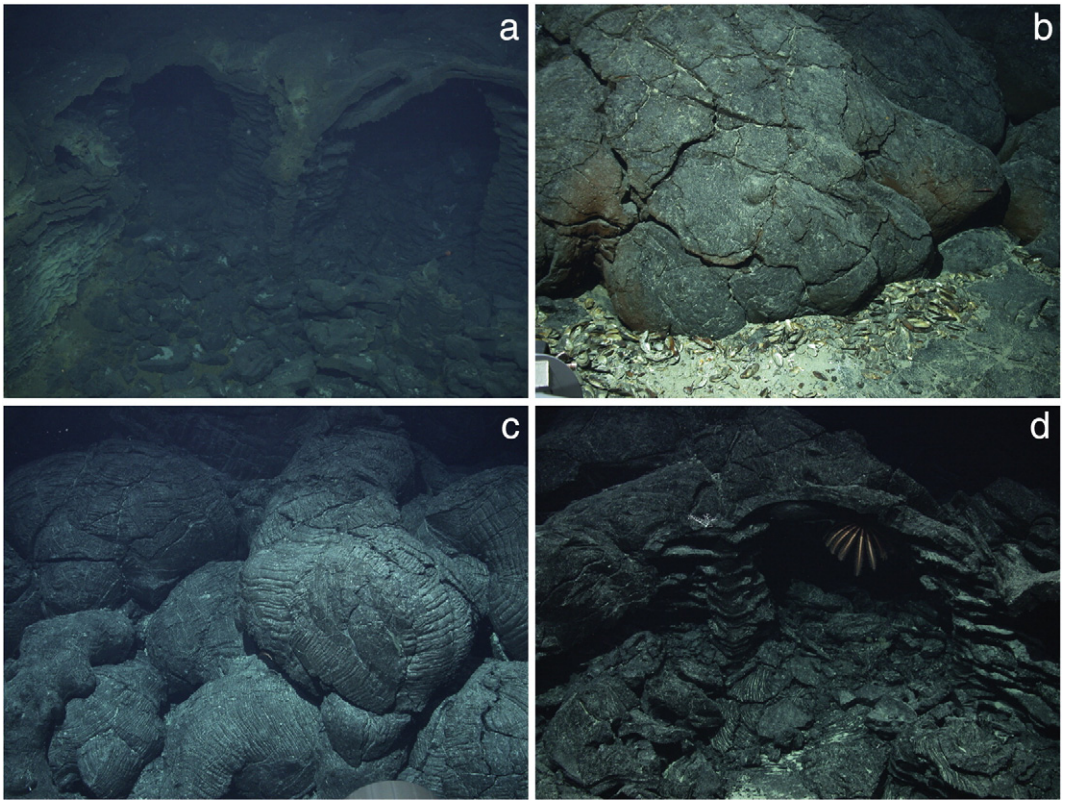

Fig. 7. Photographs of (a) hydrothermally active young lava pillars and collapse structures (Roman City site). Field of view: ~5 m, (b) pillow lava with little sediment and mussel shells (*Bathymodiolus puteoserpentis*) (Main Lilliput site). Field of view: ~1 m, (c) fresh pillow lavas, and (d) lava pillars and collapse structures in young lava flows (both in southern part of the Lilliput lava flow). Field of view: ~3 m in both images. Copyright MARUM, University of Bremen, Germany.

Fissure eruptions frequently begin with massive lava outpouring along the whole fissure followed by localization to a few main vents as the magma supply wanes (Wadge, 1981). Thus the extensive lobate and sheet lava flows probably formed early in the sequence of eruptions whereas the small pillow mounds are interpreted to reflect the closing stage of the lava eruption. Fig. 9 is a schematic diagram of the vent sites and volcanic features and shows the assumed location of fissures above the dike and eruption vents together with the lava flows connected to the separate fissures. The hydrothermal vents are located east of the supposed dike and the ascent of hot fluids occurs on the flank of the dike which probably represents the source of the heat.

The presence of the low-temperature hydrothermal Lilliput field on the A3 segment indicates that hydrothermal activity occurs on slow-spreading segments with a thickened crust. In general, magma lenses of slow-spreading ridges lie at greater depth than on faster spreading regimes (Phipps Morgan and Chen, 1993) but thermobarometric calculations of crystal fractionation processes in the A3 segment imply a relatively shallow (100–300 MPa) melt reservoir in the crust (Almeev et al., 2008). Numerical modelling suggests that in ~10-km thick crust similar to segment A3 and at typical hydrothermal cooling rates (Nusselt number ~8) a magma lens may lie deeper than 5 km (Chen, 2003) and thus may be too deep to be reached by seawater circulation. However, in the case of the Lilliput field, the hydrothermal activity is most likely caused by a diking and eruption event that affected a large part of the A3 segment. A deep magma reservoir in the crust apparently does not play a significant role in providing heat for the hydrothermal circulation. The situation of the Lilliput vents resembles that of the Rosebud vents at 86°W on the intermediate-spreading Galapagos Spreading Centre where several low-temperature vents are also known to exist and the fauna is in an early stage of development (Shank et al., 2003). The age of the Lilliput lavas appears to be much younger than 100 years because of the lack of sediment cover and freshness of the glass. Diking and eruption probably occurs more frequently on slow-spreading segments with thick crust than on segments with normal thickness because of the high magma budget. For example, detailed studies on Iceland showed eruption frequencies between 1 per 120 to 1 per 900 years (Sinton et al., 2005). Consequently, hydrothermal systems can be established for a few hundred years in thick crust whereas the large hydrothermal systems of other slow-spreading ridge segments like TAG and Snakepit are several thousand years old (Lalou et al., 1990). Fast cooling of the dike within a few weeks (Cherkaoui et al., 1997) probably generally prevents the establishment of long-lived and hot hydrothermal vent systems, however. Lower temperature, diffuse venting (such as has also been found both north and south of Iceland (German et al., 1994; Botz et al., 1999) and on the Azores Platform (Desbruyères et al., 2001)) may be more abundant along slow-spreading segments

Table 3
Measured gas compositions of the fluids from vents of the Limtoc and Lilliput sites.

Cruise/sample	Bottle	Vent area	% Fluid (Mg)	Analysed	
				H_2 nM	CH_4 nM
M68/1					
39ROV-5	KIPS-7 0.1 ml	Limtoc	7.6	26	3371
39ROV-5	KIPS-7b 0.1 ml	Limtoc	7.6	24	3371
41ROV-7	KIPS-5	Lustroc	6.6	84	1363
41ROV-11	KIPS-2	Lilliput		8	1111
70ROV-10	NISKIN 2	Roman City	9.8	136	3915
70ROV-7	KIPS-6	Roman City	6.4	260	14,206
70ROV-7	KIPS-6b	Roman City	6.4	302	14,206
70ROV-3	KIPS-3	Roman City	6.9	247	9245
70ROV-3	KIPS-3b	Roman City	6.9	204	9245
M64/1					
200ROV	Fs#15	Main Lilliput	10	16	2443
200ROV	Fs#14	Main Lilliput		16	2768

Table 4
Major element compositions of the volcanic glasses as determined by electron beam microprobe recovered from the area of the Lilliput hydrothermal field.

Sample	Latitude °S	Longitude °W	Water depth (m)	SiO_2	TiO_2	Al_2O_3	FeO^T	MnO	MgO	CaO	Na_2O	K_2O	P_2O_5	Total	K/Ti
Lilliput hydrothermal field															
M68/1 41ROV-14	9.544	13.208	1505	50.66	2.64	14.33	12.58	0.21	5.96	10.32	3.21	0.44	0.25	100.59	0.23
M64/1 200ROV-12	9.545	13.209	1495	49.51	2.49	13.60	12.07	0.23	5.45	9.91	3.36	0.45	0.40	98.06	0.25
M64/1 203VSR	9.545	13.211	1509	49.89	2.67	13.57	12.66	0.24	5.16	9.45	3.50	0.45	0.43	98.64	0.23
M64/1 213GTV-1	9.547	13.209	1513	49.81	2.40	13.84	11.81	0.20	5.61	10.15	3.31	0.43	0.40	98.55	0.25
M64/1 214GTV-1	9.547	13.209	1511	50.42	2.39	13.92	11.87	0.23	5.74	10.20	3.32	0.44	0.40	99.49	0.25
M64/1 209GTV-1	9.548	13.209	1511	50.13	2.47	13.87	11.99	0.21	5.61	10.12	3.29	0.44	0.40	99.11	0.25
M64/1 200ROV-3	9.548	13.212	1505	49.79	2.55	13.81	12.47	0.24	5.42	9.81	3.19	0.44	0.41	98.73	0.24
M64/1 200ROV-6	9.549	13.209	1496	49.79	2.78	13.66	12.30	0.20	3.81	10.25	3.47	0.51	0.43	97.89	0.25
M68/1 39ROV-6A	9.549	13.209	1494	50.70	2.57	14.38	12.13	0.21	5.72	10.18	3.14	0.44	0.26	99.73	0.24
M68/1 39ROV-7B	9.549	13.209	1494	49.60	2.71	13.94	13.75	0.24	5.96	10.21	3.34	0.41	0.22	100.39	0.21
M68/1 70ROV-8B	9.549	13.209	1496	51.09	2.74	14.31	12.00	0.21	5.76	10.11	3.19	0.43	0.24	100.08	0.22
M64/1 204VSR	9.550	13.206	1518	50.35	2.45	13.80	11.94	0.22	5.64	10.15	3.31	0.44	0.40	99.27	0.25
M68/1 33VSR-1	9.552	13.209	1479	50.95	2.83	14.09	12.78	0.22	5.16	9.38	3.26	0.48	0.32	99.47	0.23
M68/1 70ROV-4	9.552	13.207	1495	49.10	2.80	13.95	13.65	0.23	5.90	10.20	3.34	0.41	0.23	99.80	0.20
M68/1 39ROV-2	9.552	13.207	1486	50.51	2.46	14.37	11.95	0.21	5.88	10.15	3.16	0.41	0.25	99.35	0.23
Lavas south and north of Lilliput															
M68/1 36VSR-1	9.532	13.213	1477	50.90	2.67	14.09	12.24	0.21	5.47	9.89	3.14	0.47	0.30	99.37	0.25
M64/1 202VSR	9.542	13.212	1512	49.59	2.35	13.79	11.84	0.22	5.74	10.07	3.32	0.42	0.38	98.23	0.25
M64/1 205VSR	9.558	13.209	1497	50.13	2.41	13.76	12.03	0.22	5.62	10.01	3.38	0.44	0.40	98.98	0.25
M68/1 31VSR-1	9.562	13.207	1476	50.08	2.48	14.39	11.50	0.21	5.94	10.12	3.03	0.44	0.26	98.44	0.25
M64/1 210VSR	9.564	13.208	1482	50.22	2.45	13.88	11.90	0.21	5.63	10.19	3.31	0.43	0.40	99.17	0.24
M68/1 30VSR-1	9.565	13.205	1456	50.98	2.62	14.15	12.22	0.22	5.55	9.96	3.14	0.44	0.27	99.55	0.23
M64/1 211VSR	9.569	13.209	1488	49.86	2.33	13.95	11.64	0.22	5.91	10.15	3.29	0.42	0.38	98.70	0.25
M64/1 194ROV-11	9.573	13.208	1470	50.06	2.29	13.87	11.62	0.20	5.93	10.15	3.31	0.43	0.38	98.79	0.26
M64/1 194ROV-12	9.573	13.206	1460	50.32	2.34	13.93	11.76	0.19	5.75	10.22	3.29	0.43	0.39	99.17	0.26
M64/1 194ROV-13	9.573	13.206	1468	49.24	1.98	14.10	11.75	0.21	6.35	10.81	3.16	0.31	0.31	98.71	0.21
M64/1 212VSR	9.576	13.207	1413	50.10	2.40	13.76	11.79	0.23	5.70	10.16	3.29	0.42	0.40	98.80	0.24
Mean				50.15	2.51	13.97	12.16	0.22	5.63	10.09	3.27	0.43	0.34		
Si				1.07	0.38	0.48	1.11	0.03	0.90	0.53	0.21	0.07	0.14		
Pi				1.21	0.04	0.35	0.19	0.01	0.14	0.05	0.10	0.01	0.08		
HI = 5.14															
Older lavas															
M64/1 194ROV-1	9.573	13.216	1454	50.32	1.35	15.31	8.67	0.18	8.09	12.22	2.41	0.22	0.25	99.36	0.22
M64/1 194ROV-4	9.573	13.214	1429	50.35	1.16	15.56	10.04	0.18	7.93	10.57	2.67	0.08	0.18	99.02	0.09
M64/1 194ROV-6	9.573	13.213	1436	50.35	1.17	15.45	10.16	0.16	7.80	10.56	2.67	0.08	0.18	98.92	0.09
M64/1 194ROV-7	9.573	13.211	1448	50.04	1.31	15.24	8.58	0.18	8.17	12.19	2.42	0.21	0.23	98.92	0.22
M64/1 194ROV-8	9.574	13.209	1465	50.61	1.32	15.40	8.72	0.17	8.05	12.21	2.63	0.20	0.23	99.90	0.20
M64/1 194ROV-9	9.574	13.209	1465	49.68	1.29	15.38	8.48	0.16	8.14	12.17	2.41	0.21	0.24	98.50	0.23
M64/1 194ROV-10	9.573	13.208	1470	50.58	1.64	14.27	10.27	0.19	7.04	11.43	2.63	0.21	0.27	98.96	0.18
M64/1 200ROV-1	9.55	13.215	1469	50.55	2.92	13.54	12.62	0.24	4.06	8.35	3.88	0.81	0.61	98.16	0.38
M64/1 200ROV-2	9.549	13.213	1523	49.95	2.90	13.40	13.08	0.22	4.72	9.06	3.64	0.64	0.50	98.77	0.30

HI, Si and Pi according to Rubin et al. (2001).

with high magma supply and thick crust. Frequent volcanic eruptions (which will also cover vents) and magma intrusion into the very shallow crust may also contribute in preventing the formation of long-lived high-temperature vents. In contrast, lower magma production in segments with thin crust may allow the formation of stable hydrothermal systems which mine heat from deep magma bodies in the deeper crust (Wilcock and Delaney, 1996).

5.4. Implications of the biological observations

The fauna of the Lilliput vents was dominated by juvenile mussels of less than 3 cm shell length and the abundance of post-settlement stage individuals <1 mm was always high for the entire period of observation between 2005 and 2009. In contrast, the numbers of adult animals seemed to be marginal in all three visits, and large individuals of sizes around 10 cm shell length which usually dominate the appearance of mature communities at other MAR vent sites were rare. One reason for this unusual size distribution could be that Lilliput mussels grow slower and possibly also less large than mussels at other MAR vent sites. Slow growth could be due to constantly low concentrations of energy-rich volatiles in the fluids used for primary production by the mussel symbionts. However, this is not supported by our Lilliput fluid chemistry data and it is also opposed by the large colonization success of juveniles. Alternatively, it is feasible that Lilliput mussels belong to a genetically separated population that grow slower than other *Bathymodiolus*. Further investigations of MAR *Bathymodiolus* population genetics along the entire MAR will elucidate this.

On the other hand, the lack of large individuals can also reflect recurrent events of high mortality as an effect of local periodically shutdown of hydrothermal fluid supply. Periodic cessation of hydrothermal fluid supply may regularly cause death to large parts of the mussel population, while restarting hydrothermal fluid flow may strongly support larval settlement and lead to a rejuvenated mussel population, given that the supply with larvae e.g. from neighbouring vent fields is sufficient. Regional species extinction events following a shutdown of hydrothermal activity on MAR vents has been described previously (Van Dover, 1995), and pulses in hydrothermal activity would also be in agreement with the inactive Fe-oxyhydroxide mounds on the in Lilliput pillow lavas. Such a scenario could also explain why empty shells were only found at hydrothermally inactive sites but not among the thriving mussel populations within the active fluid flow. In contact to diffuse hydrothermal vent fluids, the calcite and aragonite fractions of mussel shell calcium carbonate can dissolve at rates of up to 86 μm yr^{-1} and 312 μm yr^{-1}, respectively (Lutz et al., 1994; Kennish and Lutz, 1999). Similar dissolution rates may dissolve

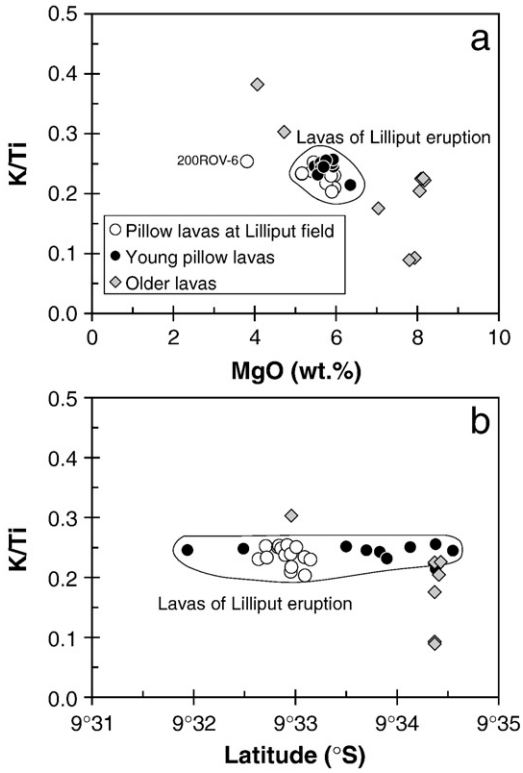

Fig. 8. Variation of (a) K/Ti ratios in the glasses versus MgO concentrations and (b) variation of K/Ti versus latitude in a part of segment A3. Note the homogeneity in K/Ti and MgO of pillow lavas sampled at the hydrothermal vents of the Lilliput field and the surrounding young pillow lavas between 9°31.9′S and 9°34.5′S suggesting the presence of a single lava flow covering this region. In contrast, older lavas sampled by ROV have different compositions.

the calcium carbonate of ~0.5 mm thick shells of *Bathymodiolus* sp. in reactivated Lilliput vents within less than two years. Young hydrothermal vent mussels at the Galapagos Spreading Centre and the North Fiji Basin showed growth rates of 2.5–3 cm in their first year of living (Rhoads et al., 1981; Schoene and Giere, 2005). If young Lilliput mussels grow at similar rates, about 90% of the mussel population in 2009 would have been less than 1 year old. Therefore the age structure of the mussel population in 2009 and also the absence of empty shells at active vent sites could indicate a possible shutdown and subsequent reactivation of hydrothermal fluid flow between 2006 and 2009. Unlike other diffuse vent fields which are often closely associated with high-temperature vents in their neighbourhood, no hyperthermophilic bacteria have been found in samples from the Lilliput vents (Perner et al., 2007) although the fluid chemistry suggests the presence of such fluids at deeper levels.

As a final point, the fauna at the Lilliput vents is largely similar to that observed at the hydrothermal vents at 5°S on the Mid-Atlantic Ridge (Haase et al., 2007) and, more importantly, similar to the faunas known north of the Equator, for example, at the Logatchev field at about 15°N (Gebruk et al., 2000). Consequently, there is no evidence for a faunal barrier at the Equatorial fracture zones between the northern and southern Mid-Atlantic Ridge vents and the northern faunas occur at least to 9.5°S.

6. Conclusions

Hydrothermal plume exploration and subsequent ROV dives and AUV mapping led to the discovery of the diffuse Lilliput hydrothermal field on the Mid-Atlantic Ridge at 9°33′S, presently the southernmost active hydrothermal field in the Atlantic. Four diffuse vent sites with diameters of several tens of metres were found within an extensive young lava flow at about 1500 m water depth. The lava flow has an estimated extension of 5 km × 0.6 km and the homogeneous major

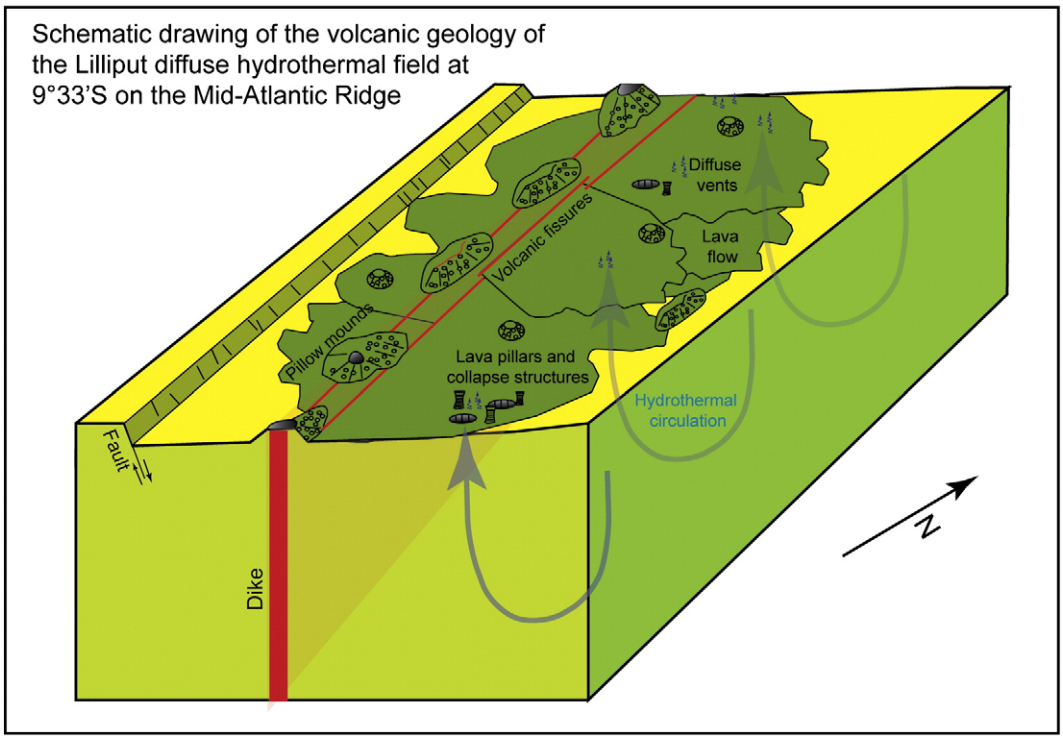

Fig. 9. Schematic drawing of the geology of the Lilliput hydrothermal field. The row of pillow mounds and small shield volcanoes forms the volcanic ridge above a thick feeder dike of the eruption. The fresh lava flow is shown in green colours whereas older lavas are in yellow. Lava tongues erupted from the series of fissures and flow fronts have been observed east of the volcanic ridge but are less clear in the west. Pillow tumuli and collapse structures occur on the lava flow. The blue arrows indicate the fluid flow and ascent of hot fluids along the flank of the supposed dike.

element composition of the recovered lavas suggests a co-magmatic relationship. The lavas probably erupted from a series of fissures along an at least 3 km long volcanic ridge which most likely represents the surface expression of a feeder dike. The four different hydrothermally active sites of the Lilliput field lie along the eastern flank of the supposed dike. Similar to findings at fast-spreading axes the hydrothermal venting of the Lilliput field appears to be related to a diking and eruption event. The fauna of the Lilliput hydrothermal field is dominated by mussels (*Bathymodiolus* sp.) of small size (<1.5 cm length) which do not show significant growth over the four years of study. This could indicate low hydrothermal activity and possibly frequent shutdown of the hydrothermal activity. The number of individuals of other species (shrimps, crabs) is limited. Diffuse hydrothermal venting appears to be typical for spreading segments with thickened crust possibly because a high magma supply rate and frequent diking and eruption events prevent the formation of stable deep-reaching hydrothermal cells. Rather, hydrothermal cooling is restricted to the uppermost crust and shallow magma intrusions.

Acknowledgments

We want to thank Captains M. Kull and W. Baschek and their crews for their help during cruises M64/1, M68/1 and M78/2 with R/V *Meteor* and the Bremen and Kiel ROV teams for their excellent work. We gratefully acknowledge the help of P. Appel, B. Mader, and N. Stroncik with the electron beam microprobe analyses and of M. Rothenbeck with postprocessing of the AUV bathymetric data. D. Teagle and an anonymous reviewer are thanked for their comments on the previous version of this manuscript. Journal reviews by W. Chadwick and an anonymous reviewer significantly improved the quality of this work. The work was supported by grants from the priority program 1144 of the Deutsche Forschungsgemeinschaft (DFG). This is publication no. 12 of the priority program 1144 "From Mantle to Ocean: Energy-, Material- and Life-Cycles at Spreading Axes" of the DFG.

References

Almeev, R.R., Holtz, F., Koepke, J., Haase, K.M., C.D., 2008. Depths of partial crystallization of H_2O-bearing MORB: phase equilibria simulations of basalts at the MAR near Ascension Island (7°–11°S). Journal of Petrology 49, 25–45.

Baker, E.T., German, C.R., 2004. On the global distribution of hydrothermal vent fields. In: German, C.R., Lin, J., Parson, L.M. (Eds.), Geophysical Monograph Series. Am. Geophys. Un., Washington, D.C., pp. 245–266.

Baker, E.T., Milburn, H.T., 1997. MAPR: a new instrument for hydrothermal plume mapping. RIDGE Events 8, 23–25.

Bischoff, J.L., Rosenbauer, R.J., 1984. The critical point and two-phase boundary of seawater, 200–500 °C. Earth and Planetary Science Letters 68, 172–180.

Botz, R., et al., 1999. Origin of trace gases in submarine hydrothermal vents of the Kolbeinsey Ridge, North Iceland. Earth and Planetary Science Letters 171, 83–93.

Brozena, J.M., 1986. Temporal and spatial variability of seafloor spreading processes in the northern South Atlantic. Journal of Geophysical Research 91, 497–510.

Bruguier, N.J., Minshull, T.A., Brozena, J.M., 2003. Morphology and tectonics of the Mid-Atlantic Ridge, 7°–12°S. Journal of Geophysical Research 108. doi:10.1029/2001JB001172.

Chadwick, W.W., Embley, R.W., 1994. Lava flows from a mid-1980s submarine eruption on the Cleft segment, Juan de Fuca Ridge. Journal of Geophysical Research 99, 4761–4776.

Chen, Y.J., 2003. Influence of the Iceland mantle plume on crustal accretion at the inflated Reykjanes Ridge: magma lens and low hydrothermal activity? Journal of Geophysical Research 108. doi:10.1029/2001JB000816.

Cherkaoui, A.S.M., Wilcock, W.S.D., Baker, E.T., 1997. Thermal fluxes associated with the 1993 diking event on the CoAxial segment, Juan de Fuca Ridge: a model for the convective cooling of a dike. Journal of Geophysical Research 102, 24887–24902.

Corliss, J.B., et al., 1979. Submarine thermal springs on the Galapagos Rift. Science 203, 1073–1083.

Delaney, J.R., et al., 1998. The quantum event of oceanic crustal accretion: impacts of diking at Mid-ocean Ridges. Science 281, 222–230.

DeMets, C., Gordon, R.G., Argus, D.F., Stein, S., 1994. Effect of recent revisions to the geomagnetic time scale on estimates of current plate motions. Geophys. Res. Lett. 21, 2191–2194.

Desbruyères, D., et al., 2001. Variations in deep-sea hydrothermal vent communities on the Mid-Atlantic Ridge near the Azores plateau. Deep-Sea Research 48, 1325–1346.

Devey, C.W., Lackschewitz, K.S., Baker, E., 2005. Hydrothermal and volcanic activity found on the southern Mid-Atlantic Ridge. Eos Transactions of the American Geophysical Union 86, 209–212.

Devey, C.W., German, C.R., Haase, K.M., Lackschewitz, K., und Melchert, B., in press. The relationships between volcanism, tectonism and hydrothermal activity in the South Atlantic. In "Diversity of hydrothermal systems on slow-spreading ocean ridges". AGU Special Volume.

Embley, R.W., Chadwick, W.W., 1994. Volcanic and hydrothermal processes associated with a recent phase of seafloor spreading at the northern Cleft segment: Juan de Fuca Ridge. Journal of Geophysical Research 99, 4741–4760.

Gebruk, A.V., Chevaldonné, P., Shank, T., Lutz, R.A., Vrijenhoek, R.C., 2000. Deep-sea hydrothermal vent communities of the Logatchev area (14°45′N, Mid-Atlantic Ridge): diverse biotopes and high biomass. Journal of the Marine Biological Association of the United Kingdom 80, 383–393.

German, C.R., Von Damm, K.L., 2003. Hydrothermal Processes, Treatise on Geochemistry. Elsevier, pp. 181–222.

German, C.R., et al., 1994. Hydrothermal activity on the Reykjanes Ridge: the Steinaholl vent-field at 63°06′N. Earth and Planetary Science Letters 121, 647–654.

Haase, K.M., et al., 2007. Young volcanism and related hydrothermal activity at 5°S on the slow-spreading southern Mid-Atlantic Ridge. Geochemistry Geophysics Geosystems 8. doi:10.1029/2006GC001509.

Haymon, R.M., et al., 1991. Hydrothermal vent distribution along the East Pacific Rise crest (9°09′–54′N) and its relationship to magmatic and tectonic processes on fast-spreading mid-ocean ridges. Earth and Planetary Science Letters 104, 513–534.

Head, J.W., Wilson, L., Smith, D.K., 1996. Mid-ocean ridge eruptive vent morphology and substructure: evidence for dike widths, eruption rates, and evolution of eruptions and axial volcanic ridges. Journal of Geophysical Research 101, 28265–28280.

Kelley, D.S., Lilley, M.D., Lupton, J.E., Olson, E.J., 1998. Enriched H_2, CH_4, and ^3He concentrations in hydrothermal plumes associated with the 1996 Gorda Ridge eruptive event. Deep-Sea Research 45, 2665–2682.

Kelley, D.S., Baross, J.A., Delaney, J.R., 2002. Volcanoes, fluids, and life at Mid-ocean Ridge spreading centers. Annual Reviews of Earth and Planetary Sciences 30, 385–491.

Kennish, M.J., Lutz, R.A., 1999. Calcium carbonate dissolution rates in deep-sea bivalve shells on the East Pacific Rise at 21°N: results of an 8-year in-situ experiment. Palaeogeography, Palaeoclimatology, Palaeoecology 154, 293–299.

Lalou, C., et al., 1990. Geochronology of TAG and Snakepit hydrothermal fields, Mid-Atlantic Ridge: witness to a long and complex hydrothermal history. Earth and Planetary Science Letters 97, 113–128.

Lutz, R.A., Kennish, M.J., Pooley, A.S., Fritz, W., 1994. Calcium carbonate dissolution rates in hydrothermal vent fields of the Guaymas Basin. Journal of Marine Research 52, 969–982.

Melchert, B., et al., 2008. First evidence for high-temperature off-axis venting of deep crustal/mantle heat: the Nibelungen hydrothermal field, southern Mid-Atlantic Ridge. Earth and Planetary Science Letters 275, 61–69.

Minshull, T.A., Bruguier, N.J., Brozena, J.M., 1998. Ridge–plume interactions or mantle heterogeneity near Ascension Island? Geology 26, 115–118.

Perner, M., et al., 2007. Microbial CO_2 fixation and sulfur cycling associated with low-temperature emissions at the Lilliput hydrothermal field, southern Mid-Atlantic Ridge (9°S). Environmental Microbiology 9, 1186–1201.

Phipps Morgan, J., Chen, Y.J., 1993. Dependence of ridge-axis morphology on magma supply and spreading rate. Nature 364, 706–708.

Rhoads, D.C., Lutz, R.A., Revelas, E.C., Cerrato, R.M., 1981. Growth of bivalves at deep-sea hydrothermal vents along the Galapagos Rift. Science 214, 911–913.

Rubin, K.H., et al., 2001. Geochemical heterogeneity within mid-ocean ridge lava flows: insights into eruption, emplacement and global variations in magma generation. Earth and Planetary Science Letters 188, 349–367.

Ruddiman, W.F., Janecek, T.R., 1989. Pliocene–Pleistocene biogenic and terrigenous fluxes at Equatorial Atlantic sites 662, 663, and 664. In: Ruddiman, W.F., Sarnthein, M., et al. (Eds.), Proceedings of the Ocean Drilling Program, Scientific Results. Ocean Drilling Program, College Station, TX, pp. 211–240.

Schoene, B.R., Giere, O., 2005. Growth increments and stable isotope variation in shells of the deep-sea hydrothermal vent bivalve mollusk *Bathymodiolus brevior* from the North Fiji Basin, Pacific Ocean. Deep-Sea Research 52, 1896–1910.

Shank, T., et al., 2003. Deep submergence synergy: Alvin and ABE explore the Galápagos Rift at 86°W. Eos Transactions of the American Geophysical Union 84, 425–440.

Singh, S.C., et al., 2006. Discovery of a magma chamber and faults beneath a Mid-Atlantic Ridge hydrothermal field. Nature 442, 1029–1032.

Sinton, J.M., Grönvold, K., Sæmundsson, K., 2005. Postglacial eruptive history of the Western Volcanic Zone, Iceland. Geochemistry Geophysics Geosystems 6. doi:10.1029/2005GC001021.

Sturm, M.E., Goldstein, S.J., Klein, E.M., Karson, J.A., Murrell, M.T., 2000. Uranium-series age constraints on lavas from the axial valley of the Mid-Atlantic Ridge, MARK area. Earth and Planetary Science Letters 181, 61–70.

Swift, J., 1726. Travels into several remote nations of the world in four parts. By Lemuel Gulliver, first a surgeon and then a captain of several ships. London.

Topsent, E., 1909. Etude sur quelques *Cladorhiza* et sur *Eucheliplura pristina* n. g. et n. sp. Bulletin de l'Institut Océanographique, Monaco 151, 1–23.

Van Dover, C.L., 1995. Ecology of Mid-Atlantic Ridge hydrothermal vents. In: Parson, L.M., Walker, C.L., Dixon, D.R. (Eds.), Hydrothermal vents and processes. Geol. Soc. Spec. Publ. Geol. Soc. London, London, pp. 257–294.

Wadge, G., 1981. The variation of magma discharge during basaltic eruptions. Journal of Volcanology and Geothermal Research 11, 139–168.

Wilcock, W.S.D., Delaney, J.R., 1996. Mid-ocean ridge sulfide deposits: evidence for heat extraction from magma chambers or cracking fronts? Earth and Planetary Science Letters 145, 49–64.